The Astronomical Journal, 160:172 (9pp), 2020 October https://doi.org/10.3847/1538-3881/aba95f

π Earth: A 3.14 day Earth-sized Planet from K2's Kitchen Served Warm by the SPECULOOS Team

Prajwal Niraula[1], Julien de Wit[1], Benjamin V. Rackham[1,17], Elsa Ducrot[2], Artem Burdanov[1], Ian J. M. Crossfield[3], Valérie Van Grootel[4], Catriona Murray[5], Lionel J. Garcia[2], Roi Alonso[6,7], Corey Beard[8], Yilen Gómez Maqueo Chew[9], Laetitia Delrez[2,4,10], Brice-Olivier Demory[11], Benjamin J. Fulton[12], Michaël Gillon[2], Maximilian N. Günther[13,18], Andrew W. Howard[14], Howard Issacson[15], Emmanuël Jehin[4], Peter P. Pedersen[5], Francisco J. Pozuelos[2,4], Didier Queloz[5], Rafael Rebolo-López[6,7], Sairam Lalitha[16], Daniel Sebastian[2], Samantha Thompson[5], and Amaury H. M. J. Triaud[16]

[1] Department of Earth, Atmospheric and Planetary Sciences, Massachusetts Institute of Technology, 77 Massachusetts Avenue, Cambridge, MA 02139, USA
[2] Astrobiology Research Unit, University of Liège, Allée du 6 Août, 19, B-4000 Liège (Sart-Tilman), Belgium
[3] Kansas University, Department of Physics and Astronomy, 1082 Malott, 1251 Wescoe Hall Drive, Lawrence, KS 66045, USA
[4] Space Sciences, Technologies and Astrophysics Research (STAR) Institute, University of Liège, Allée du 6 Août 19C, B-4000 Liége, Belgium
[5] Cavendish Laboratory, J J Thomson Avenue, Cambridge CB3 0HE, UK
[6] Instituto de Astrofísica de Canarias, E-38205 La Laguna, Tenerife, Spain
[7] Dpto. de Astrofísica, Universidad de La Laguna, E-38206 La Laguna, Tenerife, Spain
[8] Department of Physics & Astronomy, University of California, Irvine, 4129 Frederick Reines Hall, Irvine, CA 92697, USA
[9] Instituto de Astronomía, Universidad Nacional Autónoma de México, Ciudad Universitaria, CDMX, C.P. 04510, Mexico
[10] Observatoire de l'Université de Genève, Chemin des Maillettes 51, CH-1290 Versoix, Switzerland
[11] University of Bern, Center for Space and Habitability, Gesellschaftsstrasse 6, CH-3012 Bern, Switzerland
[12] NASA Exoplanet Science Institute/Caltech-IPAC, Pasadena, CA, USA
[13] Department of Physics, and Kavli Institute for Astrophysics and Space Research, Massachusetts Institute of Technology, Cambridge, MA 02139, USA
[14] California Institute of Technology, Pasadena, CA, USA
[15] Department of Astronomy, University of California, Berkeley, Berkeley, CA 94720, USA
[16] School of Physics & Astronomy, University of Birmingham, Edgbaston, Birmingham B15 2TT, UK
Received 2020 June 9; revised 2020 July 17; accepted 2020 July 23; published 2020 September 21

Abstract

We report on the discovery of a transiting Earth-sized ($0.95R_{\oplus}$) planet around an M3.5 dwarf star at 57 pc, EPIC 249631677. The planet has a period of ~3.14 days, i.e., $\sim\pi$, with an installation of 7.45 $S_{\oplus}$. The detection was made using publicly available data from K2's Campaign 15. We observed three additional transits with SPECULOOS Southern and Northern Observatories, and a stellar spectrum from Keck/HIRES, which allowed us to validate the planetary nature of the signal. The confirmed planet is well suited for comparative terrestrial exoplanetology. While exoplanets transiting ultracool dwarfs present the best opportunity for atmospheric studies of terrestrial exoplanets with the James Webb Space Telescope, those orbiting mid-M dwarfs within 100 pc such as EPIC 249631677b will become increasingly accessible with the next generation of observatories.

Unified Astronomy Thesaurus concepts: Exoplanet detection methods (489); Transit photometry (1709)

1. Introduction

The redesigned Kepler mission, K2 (Howell et al. 2014), has been a success by adding almost 400 confirmed planets to the 2348 discovered by the original mission.[19] Building upon Kepler (Borucki et al. 2010), K2 expanded the search of planets around brighter stars, covered a wider region of sky along the ecliptic, and studied a variety of astronomical objects. Together, these endeavors have revolutionized the field of exoplanetary science by quadrupling the number of exoplanets known at the time, while K2 in particular has led to exciting discoveries, such as disintegrating planetesimals around the white dwarf WD-1145 (Vanderburg et al. 2015), multi-planet systems around bright stars like GJ 9827 (K2–135; Niraula et al. 2017; Rodriguez et al. 2018), and resonant chains of planets like the K2–138 system with five planets (Christiansen et al. 2018).

Space-based platforms such as Kepler can provide high-quality continuous monitoring of targets above the Earth's atmosphere. The simultaneous photometric monitoring of tens of thousands of stars enables finding rare configurations (e.g., WD-1145) and answering science questions regarding planetary populations that are more statistical in nature such as how unique our own solar system is, or what are the most common types of planets (e.g., Fressin et al. 2013; Fulton et al. 2017).

Ground-based facilities, on the other hand, often detect fewer planets while operating at a lower cost. These planets frequently exhibit larger signal-to-noise ratios (S/Ns) in various metrics (e.g., transmission), thereby allowing for these planets to be characterized further. One such example is the TRAPPIST-1 planetary system (Gillon et al. 2016, 2017), discovered by the TRAPPIST Ultra Cool Dwarf Transiting Survey, a prototype survey for the SPECULOOS Survey (Gillon et al. 2013). The goal of the SPECULOOS Survey is to explore the nearest ultracool dwarfs ($T_{\rm eff} < 3000$ K) for transits of rocky planets (Burdanov et al. 2018; Delrez et al. 2018; Jehin et al. 2018; D. Sebastian & M. Gillon 2020, in preparation). Although few systems are expected (Delrez et al. 2018; D. Sebastian & M. Gillon 2020, in preparation), their impact on the field will be significant as they should provide most of the temperate Earth-sized exoplanets amenable for atmospheric studies with the next generation of

[17] 51 Pegasi b Fellow.
[18] Juan Carlos Torres Fellow.
[19] https://exoplanetarchive.ipac.caltech.edu

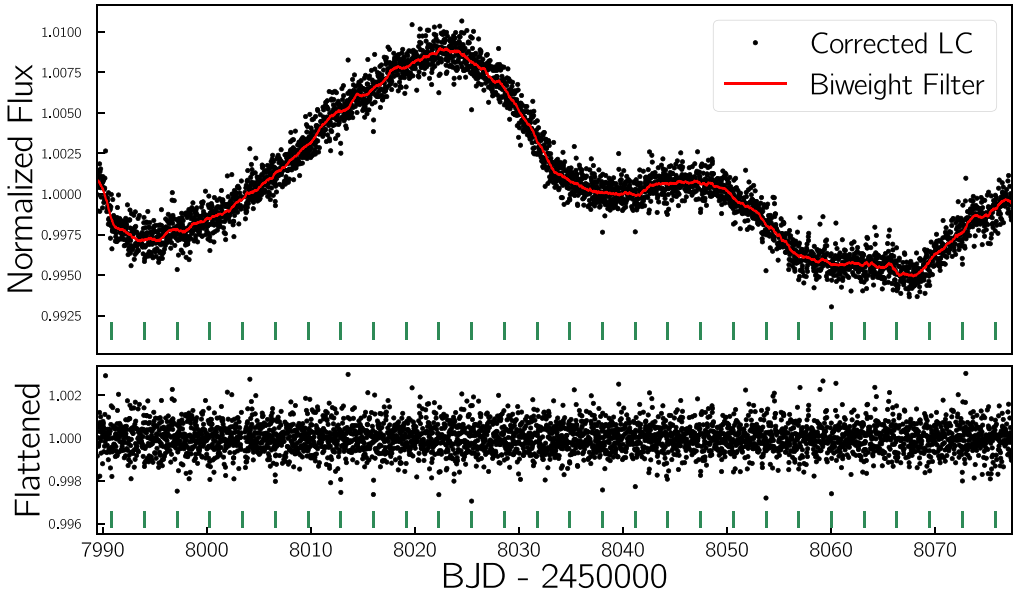

Figure 1. Upper panel: normalized curve using the detrended light curve from the `everest` pipeline of EPIC 249631677. The transits are shallow and thus not obvious. Their periodic locations are marked by green lines. The red line represents a 0.75 day biweight filter used to model out the trend in the light curve potentially due to systematics and rotational modulation of the star. Lower panel: flattened light curve used for the transit fitting, and subsequent analysis in the paper.

observatories such as the James Webb Space Telescope (JWST; e.g., Gillon et al. 2020).

Beyond the SPECULOOS Survey, which monitors nearby late-M dwarfs for terrestrial planets, the SPECULOOS telescopes have been used to study the planetary population around mid- and late-M dwarfs. In that context, SPECULOOS facilities have been involved in following up and validating planetary candidates, notably from the Transiting Exoplanet Survey Satellite (TESS; Günther et al. 2019; Kostov et al. 2019; Quinn et al. 2019). Next to confirming planetary candidates that cross detection thresholds, we have started to investigate weaker signals. For this work, we revisited K2 data, a mission that ended only in 2019. We reanalyzed the light curves of stars with $T_{\rm eff} < 3500$ K, a Kepler magnitude <15, and a $\log g > 4.5$. While these criteria were motivated particularly to look for planets around ultracool dwarfs, they were relaxed in order to allow room for errors in the stellar properties and improve completeness of the analysis. Among the 1213 stars fitting these criteria, EPIC 249631677 presented the strongest periodic transit-like signal.

In this paper, we report the discovery of an Earth-sized K2 planet in a close-in orbit around EPIC 249631677. The paper is structured as follows: observations (Section 2), analysis and validation (Section 3), and the discussion in regards to future prospects for characterization (Section 4).

2. Observations

2.1. A Candidate in Archival K2 Data

EPIC 249631677 was observed by K2 in Campaign 15 from 2017 August 23 22:18:11 UTC to 2017 November 19 22:58:27 UTC continuously for about 90 days as part of program GO 15005 (PI: I. Crossfield). The pointing was maintained by using two functioning reaction wheels, while the telescope drifted slowly in the third axis due to radiation pressure from the Sun, which was corrected periodically by thruster firing (Howell et al. 2014). As a consequence of such a modus operandi, uncorrected K2 light curves can show sawtooth structures.

Many pipelines have been built to correct for such systematics. Two popular detrending algorithms for K2 light curves are `K2SFF` (Vanderburg & Johnson 2014) and `everest` (Luger et al. 2016). These pipelines have helped to achieve precision comparable to that of Kepler by correcting for systematics caused by intra-pixel and inter-pixel variations. In the case of EPIC 249631677b, the standard deviation of the flattened light curve for `K2SFF` was observed to be 1230 ppm, compared to 685 ppm for `everest`. Considering this, we use the light curve from the `everest` pipeline, available from the Mikulski Archive for Space Telescopes, throughout this analysis. We use a biweight filter with a window of 0.75 days, as implemented in `wōtan` (Hippke et al. 2019), to generate the flattened light curve for further analysis, and use only data with quality factor of 0. This light curve can be seen in Figure 1. The simple aperture photometric light curve has a scatter of 2527 ppm, which improves to 685 ppm after `everest` processing.

We searched the flattened data for periodic transit signals using the transit least-squares algorithm (`TLS`; Hippke & Heller 2019), and found a prominent peak around 3.14 days as can be seen in Figure 2. We assessed the presence of additional candidate signals after modeling out the 3.14 day signal by re-running TLS, but did not find any with a significant signal detection efficiency (i.e., SDE > 10).

2.2. Candidate Vetting with SPECULOOS Telescopes

We followed up on the planetary candidate by observing with SPECULOOS Southern Observatory (SSO) two transit windows on UT 2020 February 25 by Ganymede and on UT 2020 March 18 by Io, and one transit window with SPECULOOS Northern Observatory (SNO) on UT 2020 May 18 by Artemis. SSO is composed of four telescopes: Io, Europa, Ganymede, and Callisto, which are installed at ESO Paranal Observatory (Chile) and have been operational since 2018 January. SNO is currently composed of one telescope (Artemis), which is located at the Teide Observatory (Canary Islands, Spain) and has been

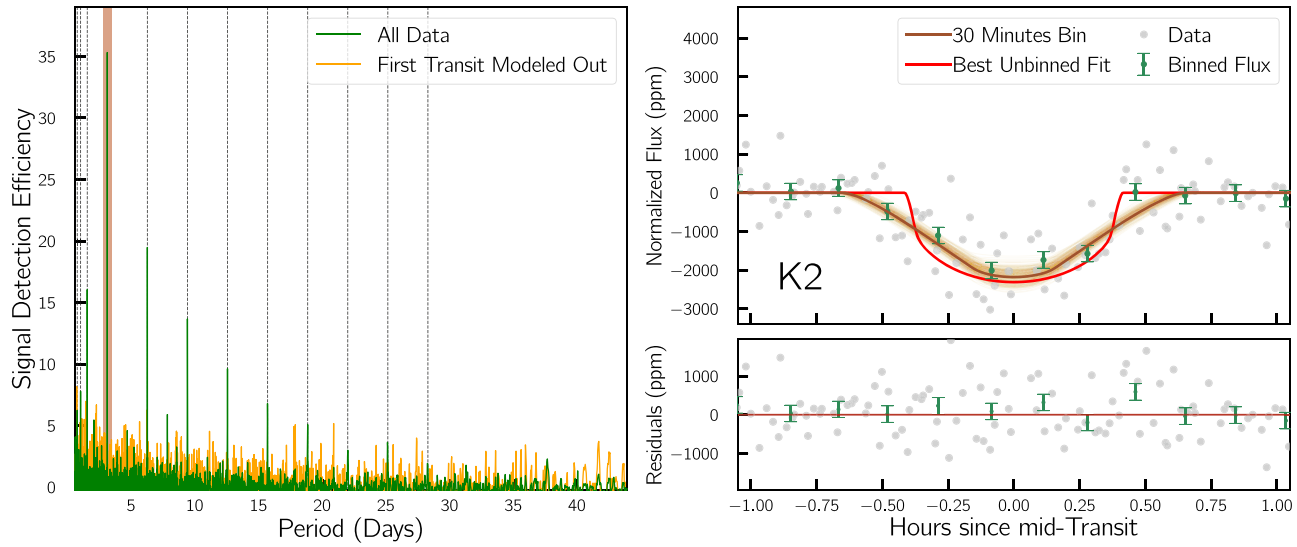

Figure 2. Left: SDE obtained from TLS showing the strongest peak at ∼3.14 days marked in red and its aliases marked with black dotted lines. No significant additional peaks were observed once the first signal was modeled out. Right: best-fit transit model for K2 data is shown in red. The brown line is the model taking into account the integration time of 29.4 minutes for K2. The orange lines illustrate 350 random models drawn from the posterior distributions of the fitted parameters.

operational since 2019 June. All SPECULOOS telescopes are identical robotic Ritchey-Chretien (F/8) telescopes with an aperture of 1 m. They are equipped with Andor iKon-L cameras with e2v 2K × 2K deep-depletion CCDs, which provide a field of view of $12' \times 12'$ and the corresponding pixel scale is $0\farcs35$ pixel^{-1} (Delrez et al. 2018; Jehin et al. 2018). To schedule those windows we used the SPeculoos Observatory sChedule maKer (SPOCK), described in D. Sebastian & M. Gillon (2020, in preparation). Observations were made with an exposure time of 40 s in an I + z filter, a custom filter (transmittance >90% from 750 nm to beyond 1000 nm) designed for the observation of faint red targets usually observed by the SPECULOOS survey (Delrez et al. 2018; Murray et al. 2020). SSO data were then processed using the SSO Pipeline, which accounts for the water vapor effects known to be significant for differential photometry of redder hosts with bluer comparison stars (Murray et al. 2020). SNO data were processed using prose, a Python-based data reduction package, which generates light curves from raw images (L. J. Garcia et al. 2020, in preparation). It creates a stacked image to extract the positions of the stars in the field, and uses the positions to perform aperture annulus photometry. A differential light curve is produced using a weighted light curve derived from the field stars, while the instrumental systematics, such as pointing shift and FWHM, are recorded to assist later in detrending. We show detrended light curves from SPECULOOS in Figure 3, where we recovered the transit events within 1σ of the calculated ephemeris from K2 data. Since these observations were obtained two years after K2 Campaign 15, they improve the precision of the transit ephemeris by an order of magnitude.

3. Analysis and Validation

3.1. Stellar Host Characterization

3.1.1. Semiempirical Stellar Parameters

We constructed the spectral energy distribution (SED) of EPIC 249631677 using photometric magnitudes from Gaia (G_{BP} and G_{RP}; Gaia Collaboration et al. 2018) and the AllWISE source catalog (J, H, K_s, $W1$, $W2$, and $W3$; Cutri et al. 2013). The corresponding fluxes for these magnitudes are tabulated on VizieR (Ochsenbein et al. 2000) and shown in Figure 4 and Table 1. The parallax of EPIC 249631677 is $\pi = 17.61 \pm 0.09$ mas, which yields a distance of 56.8 ± 0.3 pc (Gaia Collaboration et al. 2018; Stassun & Torres 2018). We then derived the stellar luminosity L_* by integrating over the SED, which yielded $L_* = 0.0041 \pm 0.0001 L_\odot$.

Two independent methods were applied to obtain stellar mass. First, we used the empirical M_*–M_{K_s} relation (applying the metallicity obtained in Section 3.1.2) from Mann et al. (2019) to obtain $M_* = 0.1721 \pm 0.0044 M_\odot$. We also applied stellar evolution modeling, using the models presented in Fernandes et al. (2019), using as a constraint the luminosity inferred above and the metallicity derived in Section 3.1.2. We considered the stellar age to be >1 Gyr in the absence of signs of youth, such as the presence of prominent flares (Ilin et al. 2019; see Section 3.1.3). We obtained with this method $M_* = 0.176 \pm 0.004\ M_\odot$. This uncertainty reflects the error propagation on the stellar luminosity and metallicity, but also the uncertainty associated with the input physics of the stellar models. We combined these two mass estimates as in van Grootel et al. (2018) to obtain $M_* = 0.174 \pm 0.004 M_\odot$ as our best estimate for the stellar mass of EPIC 249631677. Given its proximity, we expect minimal extinction (A_v) for the target; the SED fitting analysis described in Section 3.2.1 similarly constrains it to be 0.02 at 3σ confidence and we adopt that upper limit here. Finally, we note that given its luminosity, mass, and Gaia colors this star is likely to be fully convective (Jao et al. 2018; Rabus et al. 2019).

Due to the absence of a strong constraint on the stellar density from the transits, we further obtained stellar radius, surface gravity, effective temperature, and density from our evolutionary models. Table 1 summarizes the results from this analysis, along with other properties of the star. Our values are consistent with those listed in the TESS Input Catalog (Stassun et al. 2019), and we adopt them for the remainder of this analysis.

3.1.2. Reconnaissance Spectroscopy

To confirm EPIC 249631677's stellar properties and better characterize the system, we acquired an optical spectrum using

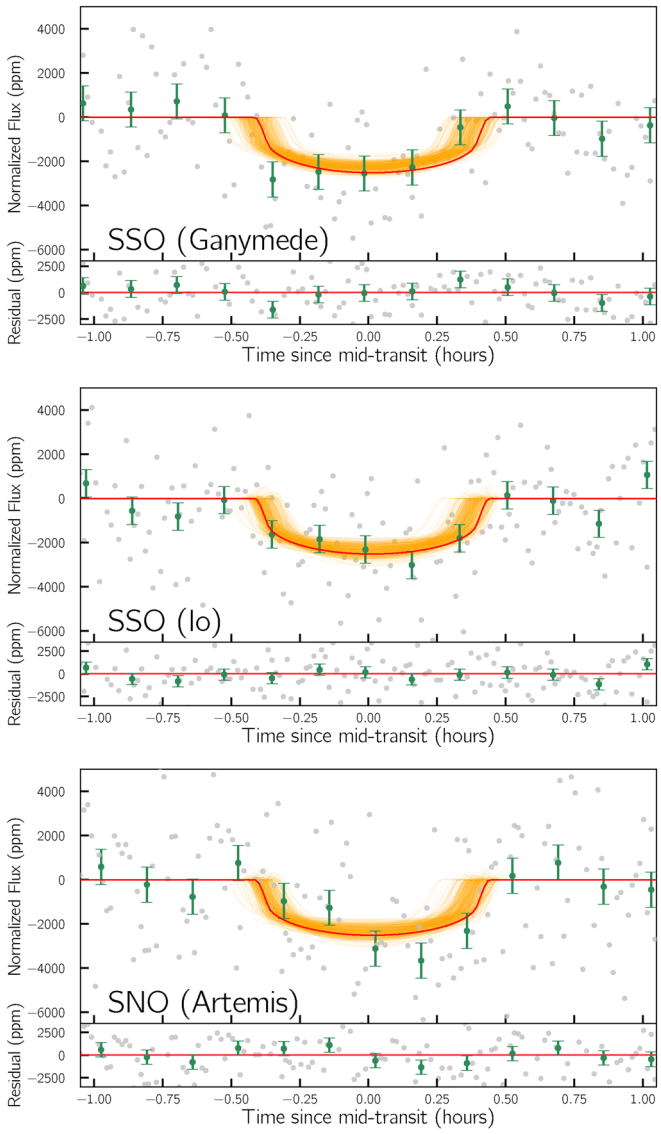

Figure 3. Top: first ground-based observation of EPIC 249631677 b from Ganymede, SSO on UT 2020 February 25 at an airmass of 1.03. Middle: second ground-based observation by Io, SSO on UT 2020 March 18 at an airmass of 1.01. Bottom: third ground-based observation by Artemis, SNO on UT 2020 May 18 at an airmass of 1.77. The best-fit model, obtained from simultaneous fitting of K2 and SPECULOOS data, is shown in red with 350 randomly selected models from MCMC posteriors shown in orange. The silver points are the detrended flux using second-order polynomials in airmass and FWHM. The green points corresponds to flux bins of 10 minutes.

Keck/HIRES (Vogt et al. 1994) on UT 2020 May 30. The observation took place in 0.″6 effective seeing and using the C2 decker without the HIRES iodine gas cell, giving an effective resolution of $\lambda/\Delta\lambda \approx 55{,}000$ from 3600 to 7990 Å. We exposed for 1800 s and obtained an S/N of roughly 23 per pixel. Data reduction followed the standard approach of the California Planet Search consortium (Howard et al. 2010).

We used our Keck/HIRES radial velocity and Gaia DR2 data to estimate the 3D galactic (*UVW*) space velocity using the online kinematics calculator[20] of Rodriguez (2016). Following Chubak et al. (2012), our Keck/HIRES spectrum gives a barycentric radial velocity of 6.25 ± 0.17 km s^{-1}. with the Gaia-derived coordinates, proper motion, and distance listed in

[20] http://kinematics.bdnyc.org/query

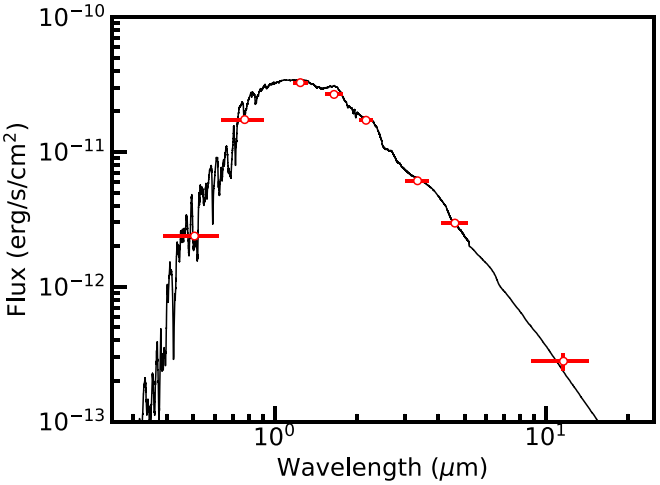

Figure 4. Spectral energy distribution of the host star. Photometric fluxes used in the stellar characterization analysis (i.e., G_{BP}, G_{RP}, J, H, K_s, $W1$, $W2$, and $W3$) are shown as points with x-errors illustrating the filter bandpasses. Flux uncertainties are generally smaller than the marker size. For comparison, a BT-Settl model spectrum (Allard et al. 2012) is shown (black line) for a star with $T_{\rm eff} = 3300$ K, $\log g = 5.0$, and [Fe/H] = 0.0, parameters similar to those derived from our SED analysis (Section 3.1.1).

Table 1, we find (U, V, W) values of (-17.02, -9.06, $+33.66$) km s^{-1}, indicating a likely membership in the Milky Way's thin disk (Bensby et al. 2014).

Using the `SpecMatch-Empirical` algorithm (Yee et al. 2017), we derive from our HIRES spectrum stellar parameters of $T_{\rm eff} = 3195 \pm 70$ K, $R_* = 0.23 \pm 0.10 R_\odot$, and [Fe/H] = -0.24 ± 0.09, consistent with the values tabulated in Table 1. The three best-matching stars in the `SpecMatch-Empirical` template library are GJ 15B, GJ 447, and GJ 725B, which have spectral types of M3.5V, M4V, and M3.5V, respectively. Given the close match between the spectra of these stars and our target (see Figure 5), we therefore classify EPIC 249631677 as an M dwarf with subclass 3.5 ± 0.5. We see no evidence of emission line cores at Hα, consistent with our determination that our target is not a young star. We see no evidence of spectral broadening compared to these three stars (which all have $v \sin i < 2.5$ km s^{-1}; Reiners et al. 2012), so we set an upper limit on EPIC 249631677's projected rotational velocity of <5 km s^{-1}, comparable to the spectral resolution of HIRES.

3.1.3. Stellar Variability

The long-term variations apparent in the `everest` light curve (Figure 1) are not evident in light curves from other reduction pipelines (e.g., `K2SFF`). These variations likely arise from systematics and are not reliable for estimating the stellar rotation period (Esselstein et al. 2018). Similarly, no flares are apparent either in the K2 or SPECULOOS data. Flare rates peak for ~M3.5 stars in TESS data (Günther et al. 2020). However, given the long integration time of 29.4 minutes as well as a need for data processing that corrects for the sawtooth pattern, flare signals, unless very prominent, are expected to be difficult to detect in K2 long cadence data.

3.2. Vetting

In order to produce a transit depth on the level of 0.2% in the light curve of the primary target, a background eclipsing binary

Table 1
Stellar Properties

Property	Value	Source
Catalog names		
EPIC ID	249631677	1
TIC ID	70298662	2
2MASS ID	J15120519-2006307	3
Gaia DR2 ID	6255978483510095488	4
Astrometric Properties		
R.A. (J2000, hh:mm:ss)	15:12:05.19	4
Decl. (J2000, dd:mm:ss)	−20:06:30.55	4
Distance (pc)	56.8 ± 0.3	4
$\mu_{\rm R.A.}$ (mas yr^{-1})	−120.3 ± 0.2	4
$\mu_{\rm DecL.}$ (mas yr^{-1})	74.7 ± 0.1	4
Barycentric Radial Velocity (km s^{-1})	+6.25 ± 0.17	6
Photometric Properties		
B (mag)	18.656 ± 0.162	2
V (mag)	17.67 ± 0.2	2
$G_{\rm BP}$ (mag)	17.3648 ± 0.0134	4
G (mag)	15.6791 ± 0.0010	4
$G_{\rm RP}$ (mag)	14.4183 ± 0.0028	4
J (mag)	12.665 ± 0.022	5
H (mag)	12.134 ± 0.027	5
K_s (mag)	11.838 ± 0.023	5
WISE 3.4 (mag)	11.631 ± 0.024	5
WISE 4.6 (mag)	11.436 ± 0.023	5
WISE 12.0 (mag)	11.068 ± 0.156	5
Derived Fundamental Properties		
Mass, M_* ($M_\odot$)	0.174 ± 0.004	6
Radius, R_* ($R_\odot$)	0.196 ± 0.006	6
Density, ρ_* (g cm^{-3})	32.6 ± 1.0	6
Luminosity, L_* ($L_\odot$)	0.0041 ± 0.0001	6
Effective Temperature, $T_{\rm eff}$ (K)	3300 ± 30	6
Surface Gravity, $\log g$ (cgs)	5.094 ± 0.006	6
Age (Gyr)	>1	6, 8
Metallicity, [Fe/H]	−0.24 ± 0.09	7
Spectral Type	M(3.5 ± 0.5)V	7
Projected Rotation, $v \sin i$ (km s^{-1})	<5	7
Extinction, A_V	<0.02	8

Note. (1) Huber et al. (2016). (2) Stassun et al. (2019). (3) Cutri et al. (2003). (4) Gaia Collaboration et al. (2018). (5) Cutri et al. (2013). (6) This work, evolutionary model analysis. (7) This work, Keck/HIRES analysis. (8) This work, SED analysis.

producing eclipses with depths of 25% to 50% would have to be 5.25–6.0 mag fainter than the target, respectively. Qualitatively, the odds of EPIC 249631677 hosting a planet are higher than the odds of such magnitude contrast eclipsing binary being present within the SPECULOOS aperture, given occurrence rates of M-dwarf planets (Dressing & Charbonneau 2013; Mulders et al. 2015; Hardegree-Ullman et al. 2019). A stringent quantitative constraint can be placed using the ingress/egress duration (T_{12}/T_{34}) compared to the total transit duration (T_{14}) (Seager & Mallén-Ornelas 2003, Equation (21)). Such a test yields an upper limit on the relative radius of the transiting body. By assuming equal effective surface temperatures, the lower magnitude limit Δm (corresponding to a flux difference ΔF) for a blended binary mimicking a signal of depth δ is given by

$$\Delta F = \left(\frac{1 - T_{23}/T_{14}}{1 + T_{23}/T_{14}}\right)^2$$
$$\Longrightarrow \Delta m = 2.5 \log_{10}\left(\frac{\Delta F}{\delta}\right). \quad (1)$$

Using the posterior for the transit fit (See Section 3.3), we find for EPIC 249631677 that such a background object can be fainter at most by 1.73 mag at the 3σ level. Fortunately, EPIC 249631677 has a significant proper motion, ∼140 mas yr^{-1}, which allows us to investigate the presence of background sources at its current sky position. We looked at archival imaging of EPIC 246331677 going back to 1953.[21] A POSS I plate from 1953 is the publicly available oldest image of EPIC 249631677, and it does not show any background source at the current position of the target as shown in Figure 6. The plate is sensitive to objects at least 3.5 magnitudes fainter than the target. Similarly, the Hubble Guide Star Catalog (GSC), with a limiting magnitude of 20 (Lasker et al. 1990), does not show any background source. While POSS II would go the deepest in terms of limiting magnitude (20.8; Reid et al. 1991), the star has moved appreciably closer to its current location, precluding a definitive measurement from this image. Overall, using archival images we can rule out the possibility of the transit signal originating from a background star at a high level of confidence.

3.2.1. Binarity of the Host Star

Despite the lack of background sources, the host star could produce a false-positive transit signal if it were a grazing eclipsing binary or a hierarchical eclipsing binary. We investigated the evidence for host star binarity using the `isochrones` software package (Morton 2015), which performs isochrone fitting in the context of the MESA (Paxton et al. 2011, 2013, 2015) Isochrones and Stellar Tracks database (Dotter 2016; Choi et al. 2016). Single-star and binary evolutionary models are available within `isochrones`, and the inference is performed via the nested sampling algorithm MULTINEST (Feroz et al. 2009; as implemented in the `PyMultiNest` software package, Buchner et al. 2014), which allows for direct comparisons of the Bayesian evidence $\ln Z$.

We tested both single-star and binary models using the priors on photometric magnitudes and stellar distance described in Section 3.1.1. The inferred properties from the single-star model fit are consistent with those given in Table 1 at the 2σ level. The $\ln Z$ for the single-star model is -213.86 ± 0.04, whereas the $\ln Z$ for the binary model is -229.6 ± 0.2. According to Kass & Raftery (1995), the corresponding Bayes factor of 16 indicates "decisive" evidence in favor of the single-star model.

We also examined our Keck/HIRES spectrum for secondary lines that would indicate the presence of another star following the approach of Kolbl et al. (2015). We found no evidence of additional lines down to the method's standard sensitivity limit of $\Delta V = 5$ mag for $\Delta v > 10$ km s^{-1}, consistent with EPIC 249631677 being a single, isolated star. We therefore conclude that the available data strongly support EPIC 246331677 being a single star.

[21] http://stdatu.stsci.edu/cgi-bin/dss_form

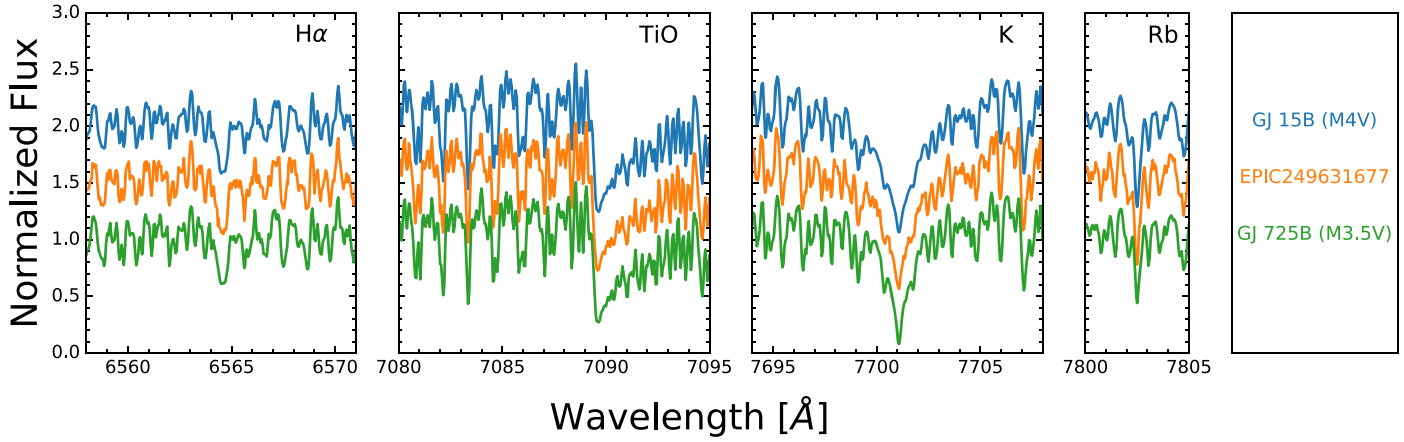

Figure 5. Comparison of Keck/HIRES spectra of EPIC 249631677 (orange) with GJ 725B (green) and GJ 15B (blue) in the vicinity of the expected locations of Hα, TiO bands, K I (7701.0 Å), and Rb I (7802.4 Å). No secondary spectral lines, emission lines, or rotational broadening are detected.

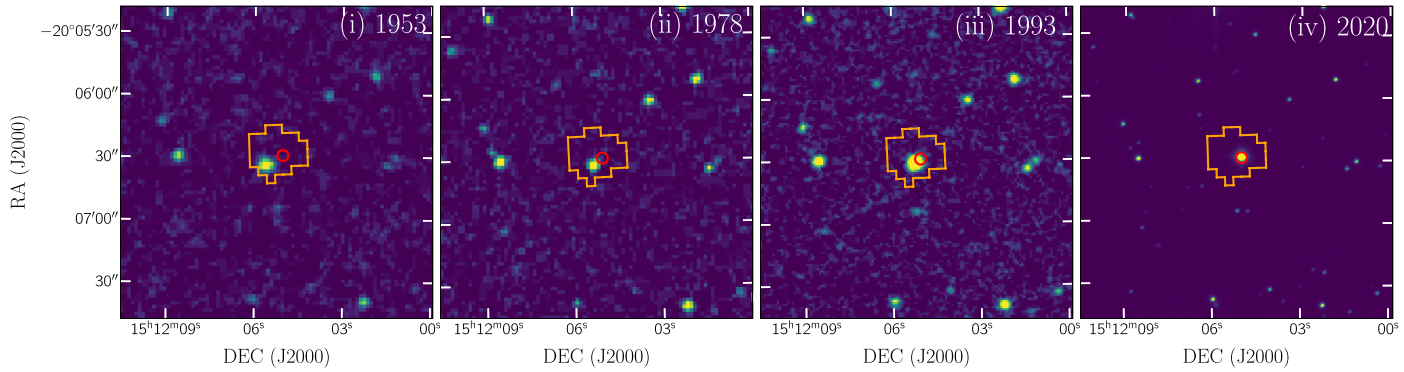

Figure 6. Set of archival images used to check for background objects. The orange polygon represents the aperture used in K2 by the `everest` pipeline, while the red circle represents the aperture used for extracting photometry using SNO. (i) POSS I Survey image from 1953 does not shown any bright object in the current SSO aperture. (ii) Image from Hubble Guide Star Catalog 1 from 1978. (iii) Image from POSS II from 1993. (iv) Median stacked image from Artemis, SNO observation made on 2020 May 18. All three archival figures do not show any background object at the current position of EPIC 249631677.

Table 2
Transit Fit Parameters

Property	Value
Period (days)	3.1443189 ± 0.0000049
$T_0 - 2450000$ (BJD)	$7990.8620^{+0.0010}_{-0.0011}$
R_p/R_*	0.0444 ± 0.0024
Radius ($R_\oplus$)	0.950 ± 0.058
a/R_*	$25.72^{+0.16}_{-0.17}$
Inclination (deg)	$88.74^{+0.21}_{-0.16}$
b	$0.565^{+0.070}_{-0.092}$
u_1 (Kepler)	$0.80^{+0.57}_{-0.53}$
u_2 (Kepler)	$-0.12^{+0.49}_{-0.44}$
u_1 (I + z)	$0.49^{+0.54}_{-0.35}$
u_2 (I + z)	$0.06^{+0.42}_{-0.39}$
T_{14} (hr)	$0.821^{+0.047}_{-0.043}$
Instellation ($S_\oplus$)	$7.45^{+0.48}_{-0.44}$
T_{eq}[a] (K)	460 ± 5

Note.
[a] Calculated assuming a Bond albedo of 0.

3.2.2. Photometric Tests

We performed a series of tests on the photometric data to rule out false-positive scenarios. First, we performed an even–odd test on the target using K2 photometry. The even and odd transits are consistent with one another in transit depth to within 1σ. We also looked for secondary eclipses in the phase-folded light curve and found none to be present. Note that since we observe consistent signals in both the K2 and SPECULOOS data sets, we can rule out the signal originating from systematics. The transit depths in SPECULOOS observations with the I + z filter, which is redder than Kepler bandpass, are consistent with K2 transit depths within the 1σ level, keeping up with the expectation of the achromatic nature of planetary transit. Furthermore, a massive companion, such as a faint white dwarf, can be ruled out using the ellipsoidal variation, which puts a 3σ upper limit on the mass of any companions at the given orbital period of the transit signal as $\sim 100\, M_{\rm Jup}$ (Morris 1985; Niraula et al. 2018). From the transit fit, we can rule out a grazing eclipse originating from a larger transiting object (i.e., $\geqslant 2R_\oplus$) at $>3\sigma$ confidence. Together, these tests rule out the object at 3.14 days being a massive companion.

3.3. Transit Fitting

We used the refined estimates of the host properties together with a joint analysis of the K2 and SPECULOOS light curves to derive the planetary properties. In order to calculate the transit model, we used `batman` (Kreidberg 2015). We simultaneously model both the K2 observation as well as the ground-based observations with 21 parameters in a Monte Carlo Markov Chain (MCMC) framework using the `emcee`

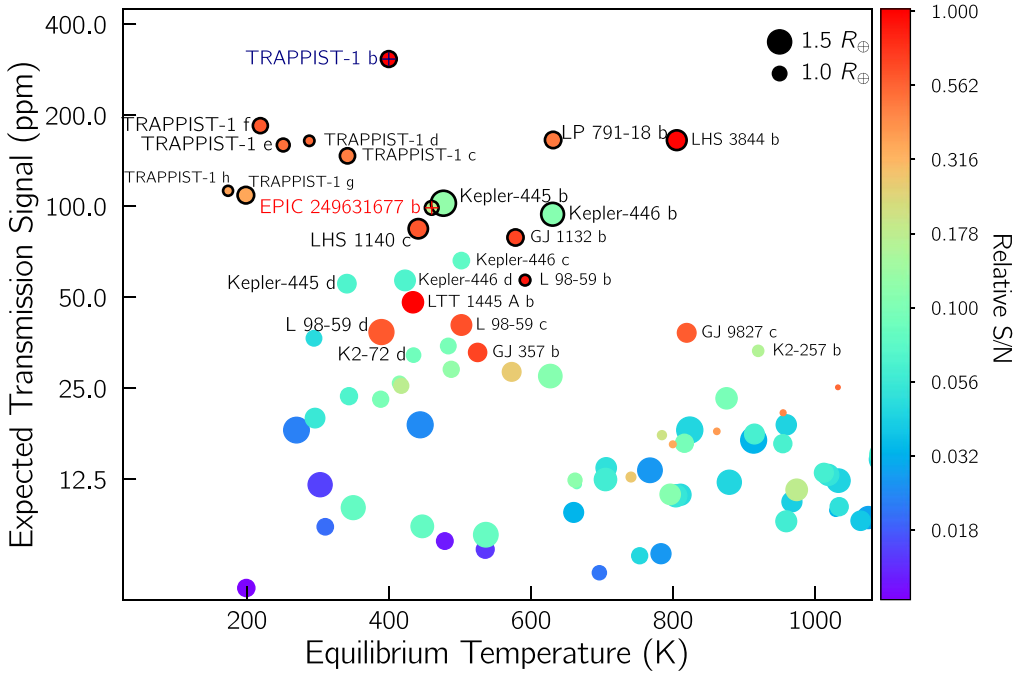

Figure 7. Most promising terrestrial planets for atmospheric characterization. Point colors illustrate the S/N of a JWST/NIRSpec observation relative to TRAPPIST-1 b. S/N below 1/100th of TRAPPIST-1b and transmission signal less than 5 ppm have been removed to enhance readability of the figure. The planets for which the presence of an atmosphere could be assessed by JWST within ∼50 transits are encircled in black, if their atmospheric signals are above JWST's threshold of ∼50 ppm. The rest of the uncircled pool of terrestrial planets may be accessible with the successors of JWST if 10 times better performance can be achieved. The size of the circle is proportional to the size of the planet. Circles for 1.5 $R_\oplus$ and 1.0 $R_\oplus$ are drawn in the upper right corner for reference.

package (Foreman-Mackey et al. 2013). We use a Gaussian prior on the scaled semimajor axis of the orbit a/R_* of $\mathcal{N}(25.72, 0.27)$, derived using Equation (30) from Winn (2010) along with the stellar density of 32.6 ± 1.0 g cm^{-3} (see Section 3.1.1) and orbital period of 3.1443 days from the TLS search. As for the limb darkening, we use the non-informative q_1, q_2 parameterization of the quadratic limb-darkening law as suggested by Kipping (2013). We fixed the eccentricity to 0, given that the expected time of circularization is 50 Myr (assuming a quality factor $Q_p \sim 500$; Goldreich & Soter 1966; Patra et al. 2017), which is at least an order of magnitude smaller than the estimated age of the system. For K2 data, we supersample the transits by a factor of 15 in `batman` to take into account the effect of nonnegligible integration time. As for the ground-based data, we use second-order polynomials to detrend against the observables airmass and FWHM.

We ran the MCMC for 50,000 steps with 150 walkers performing a combined fit of K2 and SPECULOOS data, and use the last half of the run to build the parameter posteriors. We assessed the convergence of walkers using the suggested autocorrelation test for `emcee`. The resulting median values from the fit with 1σ deviation are reported in Table 2, while the best-fit transit models are shown in Figures 2 and 3.

4. Future Prospects

The search for transiting planets around small stars has been motivated in large part by their potential for atmospheric characterization. Owing to the size and proximity of its host, EPIC 249631677b is thus one of the few known terrestrial exoplanets possibly amenable for atmospheric characterization in the next two decades. In order to quantify and contextualize its prospects for atmospheric study, we followed the same approach as for TRAPPIST-1 in Gillon et al. (2016; see de Wit & Seager 2013), focusing here on all known terrestrial planets. We selected terrestrial planets as planets with a reported radius below 1.6 $R_\oplus$ in the NASA Exoplanet Archive[22] (Rogers 2015; Fulton et al. 2017). We thus derive the amplitude of the planets' signals in transmission as

$$S = \frac{2R_p h_{\rm eff}}{R_*^2}, \text{ with}$$
$$h_{\rm eff} = \frac{7kT}{\mu g}, \quad (2)$$

where R_p is the planetary radius, R_* is the stellar radius, and $h_{\rm eff}$ is the effective atmospheric height, μ is the atmospheric mean molecular mass, T is the atmospheric temperature, and g is the local gravity. We assume $h_{\rm eff}$ to cover seven atmospheric scale heights, μ the atmospheric mean molecular mass to be 20 amu, and the atmospheric temperature to be the equilibrium temperature for a Bond albedo of 0. For the planets with missing masses, we estimated g using the model of Chen & Kipping (2017).

The signal amplitudes are reported in Figure 7 together with the S/N relative to TRAPPIST-1 b's, calculated by scaling the signal amplitude with the hosts' brightness in the J band. We find that EPIC 249631677 b fares closely to the outer planets of TRAPPIST-1 in terms of potential for atmospheric exploration with JWST—its warmer and thus larger atmosphere compensating for its larger star. In fact, its relative S/N for transmission spectroscopy is half those of TRAPPIST-1 f–h, meaning that assessing the presence of a $\mu \sim 20$ atmosphere around the planet would require of the order of 40 transits—four times the ∼10 transits required for a similar assessment for TRAPPIST-1 f–h

[22] https://exoplanetarchive.ipac.caltech.edu

(Lustig-Yaeger et al. 2019). EPIC 249631677b is thus at the very edge of JWST's capability for atmospheric characterization, mostly due to its "large" host star. The derivation above allows us to rank planets in terms of relative potential for atmospheric characterization, assuming a similar atmospheric scenario. In practice, a significant difference in atmospheric mean molecular mass, surface pressure, and/or cloud/haze altitude will strongly affect the actual potential of a planet for characterization (Lustig-Yaeger et al. 2019). For example, in some cases clouds could render the characterization of the favorable TRAPPIST-1 e difficult even with the generation of instruments following JWST (i.e., LUVOIR; Pidhorodetska et al. 2020).

With an estimated radial velocity semi-amplitude of 1.3 m s^{-1} (assuming a mass comparable to that of Earth), the planet could be accessible for mass measurements using modern ultraprecise radial velocity instruments. Such possibilities and a ranking among the 10 best-suited Earth-sized planets for atmospheric study, EPIC 249631677 b will therefore play an important role in the upcoming era of comparative exoplanetology for terrestrial worlds. It will surely be a prime target for the generation of observatories to follow JWST and bring the field fully into this new era.

This project makes use of publicly available K2 data. P.N. would like to acknowledge funding for Kerr Fellowship and Elliot Fellowship at MIT. J.d.W. and MIT gratefully acknowledge financial support from the Heising-Simons Foundation, Dr. and Mrs. Colin Masson and Dr. Peter A. Gilman for Artemis, the first telescope of the SPECULOOS network situated in Tenerife, Spain. B.V.R. thanks the Heising-Simons Foundation for support. V.V.G. is a F.R.S.-FNRS Research Associate. M.G. and E.J. are F.R.S.-FNRS Senior Research Associates. This work was also partially supported by a grant from the Simons Foundation (PI: Queloz, grant number 327127), and funding from the European Research Council under the European Union's Seventh Framework Programme (FP/2007–2013) ERC Grant Agreement Number 336480, from the ARC grant for Concerted Research Actions financed by the Wallonia-Brussels Federation, from the Balzan Prize Foundation, from F.R.S-FNRS (Research Project ID T010920F), from the European Research Council (ERC) under the European Unions Horizon 2020 research and innovation program (grant agreement No. 803193/BEBOP), and from a Leverhulme Trust Research Project Grant No. RPG-2018–418.

Facilities: Keck:I (HIRES), Kepler, MAST (HLSP, K2), SNO, SSO.

Software: `astropy` (Astropy Collaboration et al. 2013, 2018), `batman` (Kreidberg 2015), `emcee` (Foreman-Mackey et al. 2013), `isochrones` (Morton 2015), `prose` (L. J. Garcia et al. 2020, in preparation), `SPOCK` (D. Sebastian & M. Gillon 2020, in preparation), `transitleastsquares` (Hippke & Heller 2019), `wōtan` (Hippke et al. 2019).

ORCID iDs

Prajwal Niraula https://orcid.org/0000-0002-8052-3893
Julien de Wit https://orcid.org/0000-0003-2415-2191
Benjamin V. Rackham https://orcid.org/0000-0002-3627-1676
Elsa Ducrot https://orcid.org/0000-0002-7008-6888
Artem Burdanov https://orcid.org/0000-0001-9892-2406
Valérie Van Grootel https://orcid.org/0000-0003-2144-4316
Roi Alonso https://orcid.org/0000-0001-8462-8126
Corey Beard https://orcid.org/0000-0001-7708-2364
Brice-Olivier Demory https://orcid.org/0000-0002-9355-5165
Benjamin J. Fulton https://orcid.org/0000-0003-3504-5316
Michaël Gillon https://orcid.org/0000-0003-1462-7739
Maximilian N. Günther https://orcid.org/0000-0002-3164-9086
Andrew W. Howard https://orcid.org/0000-0001-8638-0320
Howard Issacson https://orcid.org/0000-0002-0531-1073
Emmanuël Jehin https://orcid.org/0000-0001-8923-488X
Peter P. Pedersen https://orcid.org/0000-0002-5220-609X
Francisco J. Pozuelos https://orcid.org/0000-0003-1572-7707
Didier Queloz https://orcid.org/0000-0002-3012-0316
Rafael Rebolo-López https://orcid.org/0000-0003-3767-7085
Sairam Lalitha https://orcid.org/0000-0001-8102-3033
Daniel Sebastian https://orcid.org/0000-0002-2214-9258
Samantha Thompson https://orcid.org/0000-0002-8039-194X
Amaury H. M. J. Triaud https://orcid.org/0000-0002-5510-8751

References

Allard, F., Homeier, D., & Freytag, B. 2012, RSPTA, 370, 2765
Astropy Collaboration, Price-Whelan, A. M., Sipőcz, B. M., et al. 2018, AJ, 156, 123
Astropy Collaboration, Robitaille, T. P., Tollerud, E. J., et al. 2013, A&A, 558, A33
Bensby, T., Feltzing, S., & Oey, M. S. 2014, A&A, 562, A71
Borucki, W. J., Koch, D., Basri, G., et al. 2010, Sci, 327, 977
Buchner, J., Georgakakis, A., Nandra, K., et al. 2014, A&A, 564, A125
Burdanov, A., Delrez, L., Gillon, M., & Jehin, E. 2018, in Handbook of Exoplanets, ed. H. Deeg & J. Belmonte (Cham: Springer), 130
Chen, J., & Kipping, D. 2017, ApJ, 834, 17
Choi, J., Dotter, A., Conroy, C., et al. 2016, ApJ, 823, 102
Christiansen, J. L., Crossfield, I. J. M., Barentsen, G., et al. 2018, AJ, 155, 57
Chubak, C., Marcy, G., Fischer, D. A., et al. 2012, arXiv:1207.6212
Cutri, R. M., Skrutskie, M. F., van Dyk, S., et al. 2003, yCat, 2246, 0
Cutri, R. M., Wright, E. L., Conrow, T., et al. 2013, yCat, 2328, 0
de Wit, J., & Seager, S. 2013, Sci, 342, 1473
Delrez, L., Gillon, M., Queloz, D., et al. 2018, Proc. SPIE, 10700, 107001I
Dotter, A. 2016, ApJS, 222, 8
Dressing, C. D., & Charbonneau, D. 2013, ApJ, 767, 95
Esselstein, R., Aigrain, S., Vanderburg, A., et al. 2018, ApJ, 859, 167
Fernandes, C. S., van Grootel, V., Salmon, S. J. A. J., et al. 2019, ApJ, 879, 94
Feroz, F., Hobson, M. P., & Bridges, M. 2009, MNRAS, 398, 1601
Foreman-Mackey, D., Hogg, D. W., Lang, D., & Goodman, J. 2013, PASP, 125, 306
Fressin, F., Torres, G., Charbonneau, D., et al. 2013, ApJ, 766, 81
Fulton, B. J., Petigura, E. A., Howard, A. W., et al. 2017, AJ, 154, 109
Gaia Collaboration, Brown, A. G. A., Vallenari, A., et al. 2018, A&A, 616, A1
Gillon, M., Jehin, E., Fumel, A., Magain, P., & Queloz, D. 2013, EPJWC, 47, 03001
Gillon, M., Jehin, E., Lederer, S. M., et al. 2016, Natur, 533, 221
Gillon, M., Meadows, V., Agol, E., et al. 2020, arXiv:2002.04798
Gillon, M., Triaud, A. H. M. J., Demory, B.-O., et al. 2017, Natur, 542, 456
Goldreich, P., & Soter, S. 1966, Icar, 5, 375
Günther, M. N., Pozuelos, F. J., Dittmann, J. A., et al. 2019, NatAs, 3, 1099
Günther, M. N., Zhan, Z., Seager, S., et al. 2020, AJ, 159, 60
Hardegree-Ullman, K. K., Cushing, M. C., Muirhead, P. S., & Christiansen, J. L. 2019, AJ, 158, 75
Hippke, M., David, T. J., Mulders, G. D., & Heller, R. 2019, AJ, 158, 143
Hippke, M., & Heller, R. 2019, A&A, 623, A39
Howard, A. W., Johnson, J. A., Marcy, G. W., et al. 2010, ApJ, 721, 1467
Howell, S. B., Sobeck, C., Haas, M., et al. 2014, PASP, 126, 398
Huber, D., Bryson, S. T., Haas, M. R., et al. 2016, ApJS, 224, 2
Ilin, E., Schmidt, S. J., Davenport, J. R. A., & Strassmeier, K. G. 2019, A&A, 622, A133

Jao, W.-C., Henry, T. J., Gies, D. R., & Hambly, N. C. 2018, ApJL, 861, L11
Jehin, E., Gillon, M., Queloz, D., et al. 2018, Msngr, 174, 2
Kass, R. E., & Raftery, A. E. 1995, J. Am. Stat. Assoc., 90, 773
Kipping, D. M. 2013, MNRAS, 435, 2152
Kolbl, R., Marcy, G. W., Isaacson, H., & Howard, A. W. 2015, AJ, 149, 18
Kostov, V. B., Schlieder, J. E., Barclay, T., et al. 2019, AJ, 158, 32
Kreidberg, L. 2015, PASP, 127, 1161
Lasker, B. M., Sturch, C. R., McLean, B. J., et al. 1990, AJ, 99, 2019
Luger, R., Agol, E., Kruse, E., et al. 2016, AJ, 152, 100
Lustig-Yaeger, J., Meadows, V. S., & Lincowski, A. P. 2019, AJ, 158, 27
Mann, A. W., Dupuy, T., Kraus, A. L., et al. 2019, ApJ, 871, 63
Morris, S. L. 1985, ApJ, 295, 143
Morton, T. D. 2015, Isochrones: Stellar Model Grid Package, Astrophysics Source Code Library, ascl:1503.010
Mulders, G. D., Pascucci, I., & Apai, D. 2015, ApJ, 814, 130
Murray, C. A., Delrez, L., Pedersen, P. P., et al. 2020, MNRAS, 495, 2446
Niraula, P., Redfield, S., Dai, F., et al. 2017, AJ, 154, 266
Niraula, P., Redfield, S., de Wit, J., et al. 2018, arXiv:1812.09227
Ochsenbein, F., Bauer, P., & Marcout, J. 2000, A&AS, 143, 23
Patra, K. C., Winn, J. N., Holman, M. J., et al. 2017, AJ, 154, 4
Paxton, B., Bildsten, L., Dotter, A., et al. 2011, ApJS, 192, 3
Paxton, B., Cantiello, M., Arras, P., et al. 2013, ApJS, 208, 4
Paxton, B., Marchant, P., Schwab, J., et al. 2015, ApJS, 220, 15
Pidhorodetska, D., Fauchez, T., Villanueva, G., Domagal-Goldman, S., & Kopparapu, R. K. 2020, ApJL, 898, L33
Quinn, S. N., Becker, J. C., Rodriguez, J. E., et al. 2019, AJ, 158, 177
Rabus, M., Lachaume, R., Jordán, A., et al. 2019, MNRAS, 484, 2674
Reid, I. N., Brewer, C., Brucato, R. J., et al. 1991, PASP, 103, 661
Reiners, A., Joshi, N., & Goldman, B. 2012, AJ, 143, 93
Rodriguez, D. 2016, Dr-Rodriguez/Kinematics-App: Stellar Kinematics, v1.0, Zenodo, doi:10.5281/zenodo.192159
Rodriguez, J. E., Vanderburg, A., Eastman, J. D., et al. 2018, AJ, 155, 72
Rogers, L. A. 2015, ApJ, 801, 41
Seager, S., & Mallén-Ornelas, G. 2003, ApJ, 585, 1038
Stassun, K. G., Oelkers, R. J., Paegert, M., et al. 2019, AJ, 158, 138
Stassun, K. G., & Torres, G. 2018, ApJ, 862, 61
van Grootel, V., Fernandes, C. S., Gillon, M., et al. 2018, ApJ, 853, 30
Vanderburg, A., & Johnson, J. A. 2014, PASP, 126, 948
Vanderburg, A., Johnson, J. A., Rappaport, S., et al. 2015, Natur, 526, 546
Vogt, S. S., Allen, S. L., Bigelow, B. C., et al. 1994, Proc. SPIE, 2198, 362
Winn, J. N. 2010, in Exoplanets, ed. S. Seager (Tucson, AZ: Univ. Arizona Press), 55
Yee, S. W., Petigura, E. A., & von Braun, K. 2017, ApJ, 836, 77